New Journal of Physics
The open-access journal for physics

Neutron scattering study of the magnetic phase diagram of underdoped $YBa_2Cu_3O_{6+x}$

D Haug[1], V Hinkov[1], Y Sidis[2], P Bourges[2], N B Christensen[3,4,5], A Ivanov[6], T Keller[1,7], C T Lin[1] and B Keimer[1,8]

[1] Max-Planck-Institut für Festkörperforschung, Heisenbergstraße 1, D-70569 Stuttgart, Germany
[2] Laboratoire Léon Brillouin, CEA-CNRS, CE-Saclay, F-91191 Gif-sûr-Yvette, France
[3] Laboratory for Neutron Scattering, ETH Zürich and Paul Scherrer Institut, CH-5232 Villigen, Switzerland
[4] Materials Research Division, Risø DTU, Technical University of Denmark, DK-4000 Roskilde, Denmark
[5] Nano-Science Center, Niels Bohr Institute, University of Copenhagen, DK-2100 Copenhagen, Denmark
[6] Institut Laue-Langevin, 6 Rue Jules Horowitz, F-38042 Grenoble Cedex 9, France
[7] ZWE FRM-II, Technische Universität München, Lichtenbergstraße 1, D-85748 Garching, Germany
E-mail: B.Keimer@fkf.mpg.de

New Journal of Physics **12** (2010) 105006 (18pp)
Received 23 July 2010
Published 29 October 2010
Online at http://www.njp.org/
doi:10.1088/1367-2630/12/10/105006

Abstract. We present a neutron triple-axis and resonant spin-echo spectroscopy study of the spin correlations in untwinned $YBa_2Cu_3O_{6+x}$ single crystals with $x = 0.3$, 0.35 and 0.45 as a function of temperature and magnetic field. As the temperature $T \to 0$, all samples exhibit static incommensurate magnetic order with propagation vector along the a-direction in the CuO_2 planes. The incommensurability δ increases monotonically with hole concentration, as it does in $La_{2-x}Sr_xCuO_4$ (LSCO). However, δ is generally smaller than in LSCO at the same doping level, and there is no sign of a reorientation of the magnetic propagation vector at the lowest doping levels. The intensity of the incommensurate Bragg reflections increases linearly with magnetic field for $YBa_2Cu_3O_{6.45}$ (superconducting $T_c = 35$ K), whereas it is field independent

[8] Author to whom any correspondence should be addressed.

for $YBa_2Cu_3O_{6.35}$ ($T_c = 10$ K). These results fit well into a picture in which superconducting and spin-density wave order parameters coexist, and their ratio is controlled by the magnetic field. They also suggest that $YBa_2Cu_3O_{6+x}$ samples with $x \sim 0.5$ exhibit incommensurate magnetic order in the high fields used for the recent quantum oscillation experiments on this system, which likely induces a reconstruction of the Fermi surface. We present neutron resonant spin-echo measurements (with energy resolution $\sim 1\,\mu$eV) for $T \neq 0$ that demonstrate a continuous thermal broadening of the incommensurate magnetic Bragg reflections into a quasi-elastic peak centered at excitation energy $E = 0$, consistent with the zero-temperature transition expected for a two-dimensional spin system with full spin–rotation symmetry. Measurements on $YBa_2Cu_3O_{6.45}$ with a conventional triple-axis spectrometer (with energy resolution $\sim 100\,\mu$eV) yield a characteristic crossover temperature $T_{SDW} \sim 30$ K for the onset of quasi-static magnetic order. Upon further heating, the wavevector characterizing low-energy spin excitations progressively approaches the commensurate antiferromagnetic wavevector, and the incommensurability vanishes in an order-parameter-like fashion at an 'electronic liquid crystal' onset temperature $T_{ELC} \sim 150$ K. Both T_{SDW} and T_{ELC} increase continuously as the Mott-insulating phase is approached with decreasing doping level. These findings are discussed in the context of current models of the interplay between magnetism and superconductivity in the cuprates.

Contents

1. Introduction

The phase diagram of the cuprate high-temperature superconductors includes three generic thermodynamic phases at zero temperature: a Mott-insulating phase with commensurate antiferromagnetic order, a d-wave superconducting (SC) phase and a metallic phase at low, intermediate and high doping levels, respectively. In the limits of zero and large doping levels, the low-energy excitations of these phases are well understood. In the Mott insulator, spin and charge excitations are separated by a large optical gap, and neutron scattering experiments have shown that the low-energy spin excitations are well described by a Heisenberg spin Hamiltonian [1, 2]. In the metallic phase at high doping levels, various transport experiments indicate that the Fermi liquid theory yields an adequate description of the coupling between spin

and charge excitations [3]–[5]. In the d-wave SC phase, however, a quantitative description of the coupling between spin and charge excitations remains a challenge for current research, and there are some indications that such a description will also answer the central question about the origin of high-temperature superconductivity.

The recent discovery of quantum oscillations in $YBa_2Cu_3O_{6+x}$ ($YBCO_{6+x}$) with $x \sim 0.5$ and in $YBa_2Cu_4O_8$ indicates that the Fermi liquid theory may also be applicable to underdoped cuprates [6]–[10], but the small size of the observed pockets is inconsistent with the large hole-like Fermi surface predicted by *ab initio* electronic structure calculations. This suggests a reconstruction of the Fermi surface by an electronic superstructure, at least in the presence of the high magnetic fields required for the quantum oscillation experiments. An incommensurate magnetic superstructure has indeed been observed in underdoped $La_{2-x}Sr_xCuO_4$ (LSCO) [11]–[14], but until recently had appeared to be a peculiar property of this family of compounds. Moreover, quantum oscillations have not yet been observed in LSCO, presumably due to a higher level of intrinsic disorder.

We recently reported a related superstructure in a $YBCO_{6+x}$ crystal with $x = 0.45$ [15], slightly below the doping level at which the quantum oscillations were observed. Although the incommensurability is about a factor of two smaller than the one in LSCO at the same doping level, this implies that incommensurate magnetic order should be regarded as another generic zero-temperature phase in the cuprate phase diagram. It remains to be established whether the incommensurate Bragg reflections observed by neutron scattering are due to a modulation of the amplitude ('stripes') [16] or the direction ('spirals') [17] of the ordered moments, or both. Nonetheless, we refer to this state as a 'spin density wave' (SDW), taking into account the observation that the incommensurate magnetic order in $YBCO_{6.45}$ develops out of a metallic state, in contrast to the commensurate antiferromagnetic order in the Mott-insulating state at lower doping levels. The amplitude of the SDW modulation is strongly enhanced by a modest magnetic field $\mathbf{H} \sim 15\,\mathrm{T}$ [18]. It is thus very likely that the same SDW state is present at the much higher fields used in the quantum oscillation experiments on crystals with slightly higher doping levels. A reconstruction of the Fermi surface by the SDW is then expected on general grounds. Subsequent work has confirmed that the size of the Fermi surface pockets observed in $YBCO_{6.5}$ can be quantitatively explained based on the incommensurate wavevector we have determined [19, 20].

An investigation of the temperature dependence of the magnetic structure and dynamics of $YBCO_{6.45}$ has revealed that the magnetic order disappears in a two-step fashion upon heating [15]. In a first step, muon spin relaxation (μSR) experiments showed that static magnetic order, which reduces the translational symmetry of the lattice, vanishes at a temperature $T \sim 2\,\mathrm{K}$. In a second step, the incommensurate wavevector characterizing low-energy magnetic fluctuations continuously approaches the commensurate antiferromagnetic ordering wavevector with increasing temperature, and the incommensurability vanishes in an order-parameter-like fashion at $T_{\mathrm{ELC}} \sim 150\,\mathrm{K}$. While the magnetic fluctuations above T_{ELC} respect the fourfold rotation symmetry of the CuO_2 plane, their wavevector spontaneously aligns with one of the two nearly equivalent copper–oxygen bond directions upon cooling below this temperature. In a wide temperature regime, therefore, the spin system collectively behaves in such a way that the rotational symmetry is broken, whereas the translational symmetry remains intact. Since the symmetry properties of this state are analogous to those of a nematic liquid crystal, we refer to this state as an 'electronic liquid crystal' (ELC) [21]. The small orthorhombicity of the $YBCO_{6.45}$ crystal lattice is required to align the ELC domains such that the ELC state

Table 1. Summary of the underdoped $YBCO_{6+x}$ samples. The SC transition temperature T_c was determined by magnetometry. The out-of-plane lattice parameter c at room temperature was determined by x-ray powder diffraction on selected samples from the same batch. From this value, the hole doping level per planar Cu ion p could be extracted [27]. Several tens of crystals were co-aligned by x-ray Laue diffractometry, mimicking a large single-domain crystal with a total mass m_{tot}.

Sample	T_c (K)	Lattice parameter c (Å)	Hole doping p	Total mass m_{tot} (g)
$YBCO_{6.45}$	35	11.761	0.082	2.0
$YBCO_{6.35}$	10	11.781	0.062	1.4
$YBCO_{6.3}$	0	11.791	0.052	1.0

becomes observable in a volume-integrating method such as neutron scattering. In the presence of this aligning field, the ELC transition is rounded into a sharp crossover. While the neutron scattering data are not accurate enough to quantify this rounding, the strong, order-parameter-like temperature dependence of the incommensurability indicates that the loss of rotational symmetry reflects an underlying phase transition that is driven by collective interactions between the spins.

Our work on $YBCO_{6.45}$ raises several questions. How is the incommensurate SDW related to the magnetic order observed in LSCO, and how does it evolve into the commensurate antiferromagnetic order [1, 22] observed in $YBCO_{6+x}$ at lower doping levels? How is the ELC state related to anomalies in the charge dynamics observed by transport (such as Nernst effect measurements [23, 24]) and spectroscopic probes (such as infrared spectroscopy [25]) in the same temperature and doping range? This paper describes neutron scattering measurements on untwinned $YBCO_{6+x}$ crystals with $x = 0.3$ and 0.35 designed to address these questions, and to constrain theoretical models of the collective magnetic ordering phenomena in the cuprates. In conjunction with measurements on $x = 0.45$ and higher doping levels, the results allow us to determine the doping dependence of the incommensurate wavevector as well as the characteristic crossover temperatures for SDW and ELC ordering in $YBCO_{6+x}$. For a $YBCO_{6.35}$ crystal, we also present data on the magnetic field dependence of the SDW order parameter at low temperatures, as well as temperature-dependent neutron resonant spin-echo experiments that bridge the gap in energy scales between μSR and conventional neutron diffraction data. The results of our study allow us to draw an outline of the phase diagram of underdoped $YBCO_{6+x}$ as a function of doping, magnetic field and temperature.

2. Experimental details

The measurements were performed on crystal arrays with three different hole-doping levels in the strongly underdoped regime of the $YBCO_{6+x}$ phase diagram. The samples are listed in table 1. The oxygen content of the single crystals was carefully adjusted by a thermal treatment during which oxygen diffusion takes place. A variation in temperature at fixed oxygen partial pressure results in different oxygen contents and thus different hole concentrations [26]. The oxygen content and hole concentration per planar Cu ion, p, were extracted from the known doping dependence of the out-of-plane lattice parameter c and T_c [27].

In $YBCO_{6+x}$, a unique axis in the CuO_2 plane is established by the orthorhombic distortion of the crystal structure. However, as-grown samples show crystallographic twinning, because the difference between the in-plane lattice parameters a and b is small. In order to observe the anisotropy of the electron system with a volume-averaging probe such as neutron scattering, a single-domain state has to be prepared in which the orientation of the two in-plane axes is maintained throughout the entire sample volume. This was accomplished by individually detwinning single crystals of $YBCO_{6+x}$ (with typical size $a \times b \times c = 2 \times 2 \times 0.5\,\mathrm{mm}^3$) by application of uniaxial mechanical stress along the crystallographic (1,0,0) direction.

The crystals were characterized by magnetometry and were found to exhibit SC transitions with widths of 2–4 K, testifying to their high quality. In order to obtain a sample volume sufficient for inelastic neutron scattering experiments, several tens of crystals were co-aligned on a single-crystalline silicon disc by x-ray Laue diffractometry. The resulting crystal arrays, mimicking large single-domain crystals, had mosaicities of $\leqslant 1.5^\circ$ and a majority twin domain population close to 90%. The contribution of the minority twin domains to the observed magnetic scattering signal is thus below the detection limit.

The neutron experiments were performed at the triple-axis spectrometers IN8 and IN14 (ILL, Grenoble, France), 4F1 and 4F2 (LLB, Saclay, France), Rita-II (SINQ, PSI Villigen, Switzerland) and on the resonant spin-echo triple-axis spectrometer TRISP (FRM-II, Garching, Germany). Pyrolytic-graphite crystals were used to monochromate and analyze the neutron beam. In order to extinguish higher-order contaminations of the neutron beam, a beryllium filter was inserted into the beam for those measurements that were performed with fixed final wavevector $k_\mathrm{f} = 1.55\,\mathrm{Å}^{-1}$. For the same purpose, a pyrolytic-graphite filter was used when measuring at $k_\mathrm{f} = 2.57\,\mathrm{Å}^{-1}$ and $k_\mathrm{f} = 2.66\,\mathrm{Å}^{-1}$, respectively. On TRISP, two radio-frequency coil sets, located between the monochromator and sample and between the sample and analyzer, were used to manipulate the Larmor phase of the neutron spin before and after the scattering event, and the relaxation rate of magnetic excitations was extracted from spin-echo profiles [28].

The scattering vector $\mathbf{Q} = (H, K, L)$ is expressed in reciprocal lattice units (r.l.u.), i.e. in units of the reciprocal lattice vectors a^*, b^* and c^* ($a^* = 2\pi/a$, etc). As in the undoped ($x = 0$) parent compound, magnetic intensity is concentrated around the antiferromagnetic wavevector $\mathbf{Q}_\mathrm{AFM} = (0.5, 0.5, L)$. Scans were thus performed either around $\mathbf{Q}_\mathrm{AFM}$ or around the equivalent points $(0.5, 1.5, L)$ and $(1.5, 0.5, L)$ in higher Brillouin zones.

For the measurements in high magnetic field, the sample was mounted on a 15 T vertical-field cryomagnet. The scattering plane was spanned by the vectors (1,0,0) and (0,1,2), and scans were performed along a^* around $\mathbf{Q} = (0.5, 0.5, 1)$. The scattering geometry implies an angle of 33° between the magnetic field $\mathbf{H}$ and the c-axis. Thus, for the field-dependent experiments, the external magnetic field has a major component perpendicular to the CuO_2 planes. All scans for $\mathbf{H} \neq 0$ were performed after field cooling.

3. Results

3.1. Doping dependence

We first discuss the behavior of the spin system at the lowest temperatures studied in our experiments ($T = 2\,\mathrm{K}$). Figure 1 shows the low-temperature neutron scattering function $S(\mathbf{Q}, \omega)$ of $YBCO_{6.35}$ around the antiferromagnetic ordering wavevector $\mathbf{Q}_\mathrm{AFM} = (0.5, 0.5, 1)$ as a function of excitation energy $E = \hbar\omega$. It is apparent that the spectrum comprises two

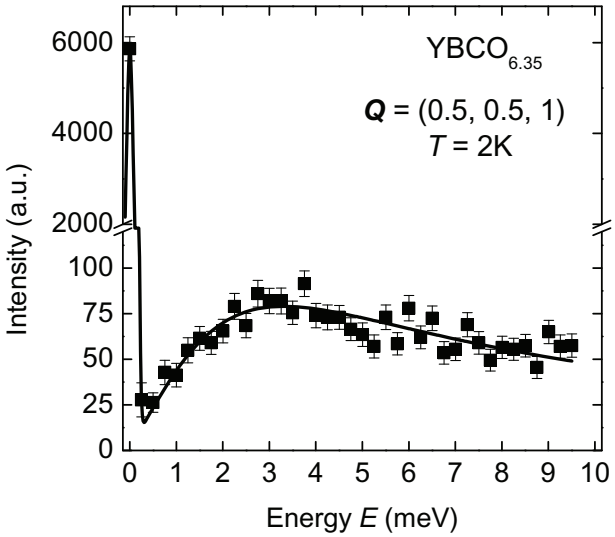

Figure 1. Magnetic neutron scattering function of $YBCO_{6.35}$ at $T = 2\,K$ and $\mathbf{Q} = (0.5, 0.5, 1)$, showing distinct quasi-elastic and inelastic components.

components: a sharp, intense 'quasi-elastic' peak centered at $E = 0$ and a weaker inelastic component that depends smoothly on energy. The two components are analogous to the Bragg peak and the spin wave spectrum of an antiferromagnetically ordered state. At the lowest temperatures, the energy width of the quasi-elastic peak is at the resolution limit of neutron resonant spin-echo spectroscopy ($\sim 1\,\mu$eV, see below), and μSR experiments indicate magnetic order that persists much longer than the muon lifetime ($\sim 2\,\mu$s). At temperatures of the order of 2 K, which includes the temperature range in which the quantum oscillation experiments were carried out, the quasi-elastic peak can therefore be regarded as a signature of static magnetic order. The two-component form of the magnetic spectrum is common to all three samples studied here[9].

In order to determine the spatial character of the magnetic correlations, we have performed constant-energy scans through the low-energy spin excitation spectrum. Figure 2 shows a comparison of constant-energy scans for $E = 3$ meV along the in-plane crystallographic directions a^* and b^* for $YBCO_{6.45}$, $YBCO_{6.35}$ and $YBCO_{6.3}$. Note that these are raw data, without any background subtraction. Scans through the quasi-elastic peak are of lower quality because they are superposed by a background due to incoherent scattering from the sample and the sample mount, but the scan profiles are nearly identical [15]. Clearly, the magnetic response of all three samples shows a pronounced in-plane anisotropy. The cuts through the $YBCO_{6.45}$ spectrum (figures 2(a) and (b)) demonstrate that the anisotropic intensity distribution is a consequence of two incommensurate peaks that are symmetrically displaced from $\mathbf{Q}_{AFM}$ along a^*, whereas the distribution is commensurate along b^*. For $YBCO_{6.35}$, the anisotropy is qualitatively similar, but less pronounced (figures 2(c) and (d)), and it is further reduced for $YBCO_{6.3}$ (figures 2(e) and (f)). Note that even in this latter case we can rule out any influence of

[9] For $YBCO_{6.3}$ and $YBCO_{6.35}$, both commensurate quasi-elastic reflections centered at integer L and incommensurate peaks with continuous L dependence characteristic of two-dimensional (2D) magnetic order are detected. Both sets of reflections exhibit a similar temperature dependence.

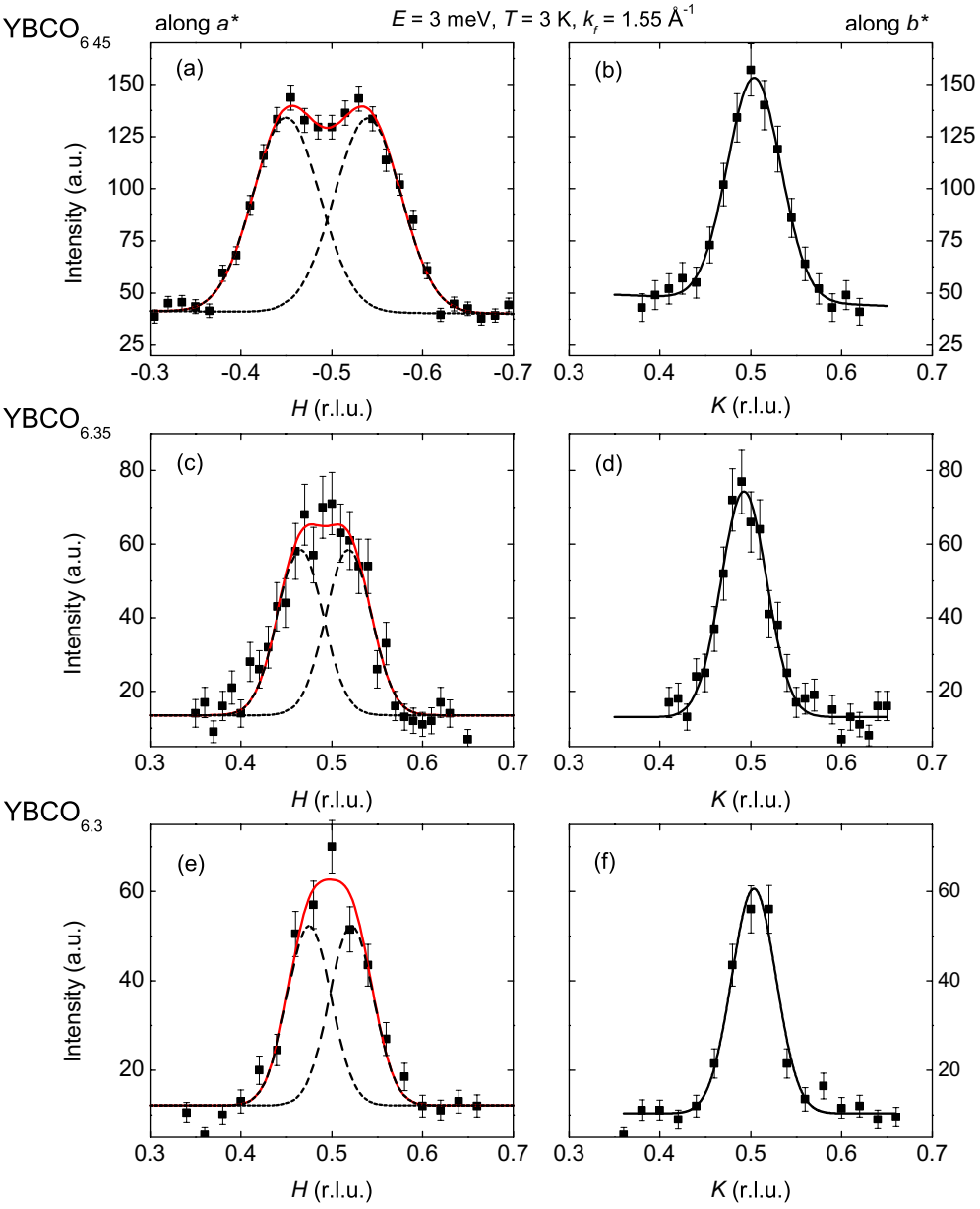

Figure 2. Constant-energy scans (raw data, without background correction) at $E = 3$ meV and $T = 3$ K along a^* and b^* for (a,b) $YBCO_{6.45}$, (c,d) $YBCO_{6.35}$ and (e,f) $YBCO_{6.3}$. The lines are single-Gaussian (b^*) and double-Gaussian (a^*) profiles fitted to the data. The two incommensurate peaks symmetrically displaced from $\mathbf{Q}_{\mathrm{AFM}}$ along a^* are shown as dashed lines.

the instrumental resolution on the anisotropic peak profile[10]. Although the splitting between the two incommensurate peaks in the a^*-direction is no longer resolved for $YBCO_{6.35}$ and $YBCO_{6.3}$, fits to two-Gaussian profiles with individual peak widths matching the one in the b^*-direction

[10] The full-width at half-maximum of the elastic resolution function was determined at $\mathbf{Q}_{\mathrm{AFM}} = (0.5, 0.5, 1)$ using the $\lambda/2$ harmonic of the Bragg reflection (1, 1, 2) by removing the filters; it is $\sim (0.025 \pm 0.002)$ r.l.u. in the a^*-direction and $\sim (0.023 \pm 0.002)$ r.l.u. in the b^*-direction. The effective inelastic resolution is somewhat larger, but still much smaller than the width of the scan profiles along both a^* and b^*.

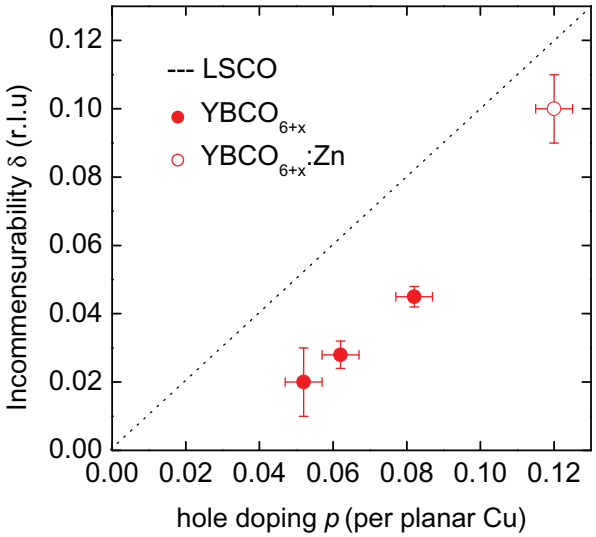

Figure 3. Doping dependence of the incommensurability δ (i.e. the displacement of the peaks from $\mathbf{Q}_{\mathrm{AFM}}$) for an energy transfer of $E = 3\,\mathrm{meV}$ at low temperatures, extracted from the fits in figure 2 (closed symbols). The open symbol denotes the incommensurability of the low-energy spin excitations for Zn-substituted $YBCO_{6.6}$ (from [29]). For comparison, the linear δ-versus-p relation for LSCO is shown as a dashed line [11, 12].

provide excellent descriptions of the data (lines in figure 2). Together with the observation of a split profile for $YBCO_{6.45}$ (figure 2(a)), this indicates an incommensurability of the magnetic response that increases continuously with increasing hole content in the CuO_2 planes.

Figure 3 summarizes the doping dependence of the incommensurability δ in the three $YBCO_{6+x}$ samples that exhibit static magnetic order. We have also included data obtained from a $YBCO_{6.6}$ sample in which static incommensurate magnetic order was induced by substituting 2% of the Cu atoms by spinless Zn impurities [29]. It is instructive to compare these data to the doping dependence of δ in the LSCO family of cuprates, where the propagation vector of the incommensurate modulation of the spin system is along the Cu–O bond direction for $p \gtrsim 0.05$, as it is in $YBCO_{6+x}$ [11, 12]. However, δ is systematically lower in $YBCO_{6+x}$ than it is in LSCO at the same p. While in LSCO a linear relationship between the incommensurability and the doping level ($\delta = p$) is observed for $p \lesssim 0.12$, δ in $YBCO_{6+x}$ extrapolates to zero as $p \to 0.04$ from above, close to the doping level at which the propagation vector switches from the Cu–O bond direction to the diagonal of a CuO_4 plaquette in LSCO [13, 14]. In contrast, we have not found any evidence for a 45° reorientation of the incommensurate modulation in $YBCO_{6+x}$ in the doping range we have investigated. Possible origins of this material-specific behavior include exchange interactions between directly adjacent copper–oxygen planes in the crystallographic unit cell (which comprises bilayer units in $YBCO_{6+x}$ and a single-layer unit in LSCO), and the lower disorder in $YBCO_{6+x}$, which allows metallic conduction at lower p than in LSCO. Calculations considering the impact of these factors in the framework of a model in which the magnetic incommensurability arises from spiral order are indeed consistent with the behavior we have observed [30] and [31].

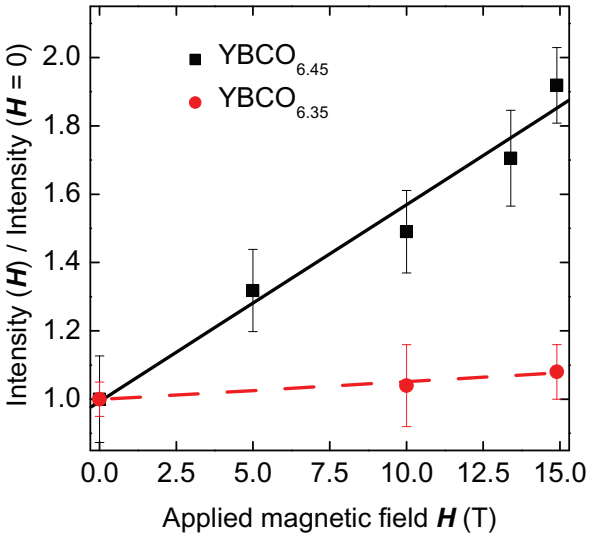

Figure 4. Magnetic field dependence of the quasi-elastic magnetic peak at $T = 2\,\mathrm{K}$ for $YBCO_{6.45}$ (reproduced from [18]) and $YBCO_{6.35}$. The data were normalized to the intensity at $\mathbf{H} = 0$.

3.2. Magnetic field dependence

As discussed in section 1, we have shown that the intensity of the quasi-elastic peak in $YBCO_{6.45}$ is strongly enhanced in an external magnetic field, while its shape is only weakly affected [18]. This effect is analogous to a similar phenomenology previously established in LSCO for $x \sim 1/8$ [32]–[34]. It is naturally explained as a consequence of a competition between SDW and d-wave SC phases, which coexist in $YBCO_{6.45}$ for $\mathbf{H} = 0$ [35]. Since the magnetic field destabilizes d-wave superconductivity by orbital depairing, the SC order parameter is reduced, and the SDW order parameter is consequently enhanced for $\mathbf{H} \neq 0$.

In order to further explore the validity of this scenario, we have extended our high-magnetic-field measurements to $YBCO_{6.35}$. Figure 4 shows the $\mathbf{H}$-dependence of the quasi-elastic peak intensity at $T = 2\,\mathrm{K}$ for the two different doping levels. Whereas the peak intensity for $YBCO_{6.45}$ increases linearly with increasing magnetic field [18], the magnetic intensity is field independent within the error bar for $YBCO_{6.35}$. The field independence is consistent with earlier observations on a twinned $YBCO_{6+x}$ sample with similar hole concentration [36] and on Nd-substituted LSCO samples in which the SDW order is already well established for $\mathbf{H} = 0$ [37]. It also fits well into a two-phase competition scenario in which the SDW phase fraction in $YBCO_{6.35}$ is already close to 100% for $\mathbf{H} = 0$.

3.3. Temperature dependence

3.3.1. Spin density wave (SDW). We now address the temperature dependence of the spin correlations, beginning with the intensity of the quasi-elastic peak. Figure 5(a) shows the temperature dependence of the quasi-elastic peak intensity of $YBCO_{6.35}$ measured on a conventional cold-neutron triple-axis spectrometer with energy resolution $\sim 0.1\,\mathrm{meV}$ (half-width at half-maximum, HWHM). The data appear to show an SDW transition at a temperature of $T_{\mathrm{SDW}} \sim 40\,\mathrm{K}$. However, the rounding of the transition, which substantially exceeds the width

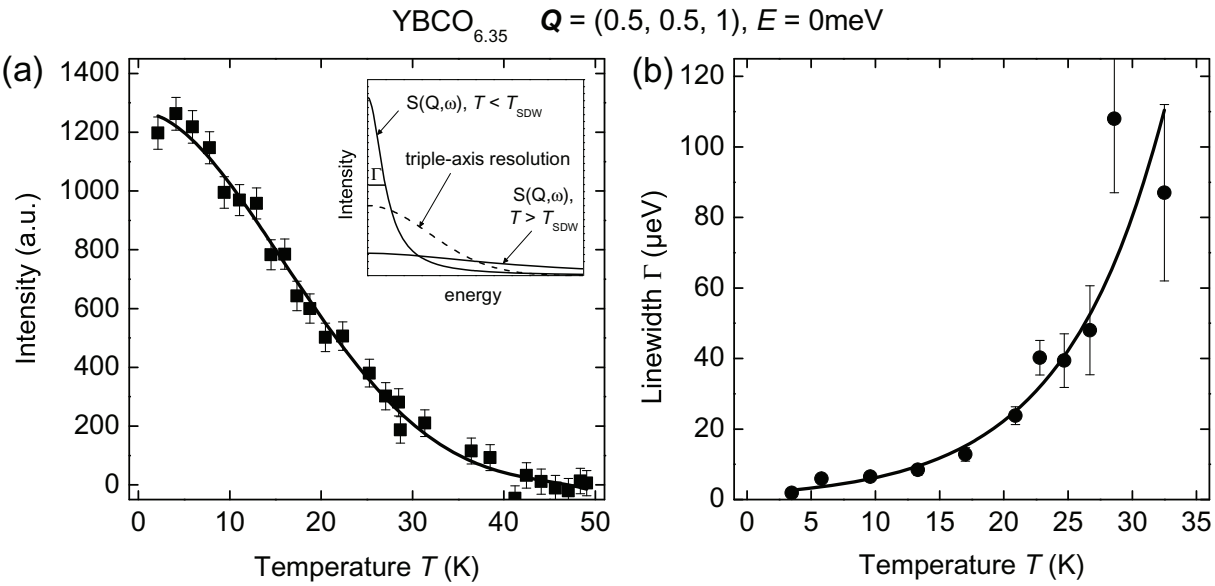

Figure 5. Intensity of the quasi-elastic peak in $YBCO_{6.35}$ determined by conventional cold-neutron triple-axis spectrometry (a) and energy width (HWHM) of the same peak determined by resonant spin-echo spectroscopy (b) as a function of temperature. The lines are guides to the eye. The inset shows a sketch of the Lorentzian lineshape of the quasi-elastic peak determined by spin-echo spectroscopy at different temperatures (solid lines) in relation to the Gaussian resolution of the triple-axis spectrometer (dashed line).

of the SC transition in these samples ($\sim$ 2–4 K), and the lack of saturation at low temperatures are unusual. Moreover, μSR experiments indicate 'spin freezing' transitions at much lower temperatures in this range of the phase diagram [15, 22, 38]. Similar observations have been reported for underdoped LSCO [39, 40].

In order to explore the origin of this behavior, we have carried out neutron resonant spin-echo measurements [28] with an energy resolution of $\sim 1\ \mu$eV, which bridge the gap in energy scales between conventional neutron diffraction and μSR. The spin-echo profiles indicate that the quasi-elastic peak exhibits a Lorentzian lineshape with an intrinsic energy width (HWHM), Γ, that exceeds the resolution of the spin-echo instrument for $T \geqslant 5$ K (figure 5(b)). Γ increases continuously with increasing temperature and exceeds the HWHM of the Gaussian resolution function of the triple-axis instrument for $T \geqslant 40$ K (the inset of figure 5(a)). These results show that the rounding observed in figure 5(a) is of dynamic origin and not due to an inhomogeneous distribution of transition temperatures as one might have suspected. They also imply that the SDW transition suggested by figure 5(a) is actually a crossover whose specific form is determined by the energy window sampled by the experimental method. For comparison with the results of transport experiments and other experimental probes of the charge dynamics, it is nonetheless useful to monitor the strength of the quasi-static SDW correlations at $T \neq 0$, which can be characterized by the crossover temperature T_{SDW} above which the width of the quasi-elastic peak exceeds the energy scale ~ 0.1 meV. We have therefore extracted this temperature from the data of figure 5(a) and analogous data collected for the other doping levels.

The diverging fluctuation time scale implied by the data of figure 5(b) is naturally explained as a consequence of the zero-temperature phase transition expected for a 2D spin system with

full spin–rotation symmetry. In this scenario, the intensity of the quasi-elastic peak for $T \to 0$ is proportional to the SDW order parameter. In contrast to the divergence of the correlation length expected for a $T = 0$ phase transition, the width of the scattering profiles in momentum space (figure 2) saturates at low temperature. This may reflect either an inhomogeneous broadening of the profiles due to slight variation of doping levels across the large single-crystal array, or finite-size effects imposed by the random distribution of dopant atoms and/or the coexistence of SDW and SC phases. We note, however, that the two-component form of the scattering function shown in figure 1 is closely similar to the spectrum of an undoped 2D square-lattice antiferromagnet at $T \neq 0$, where thermal fluctuations generate a finite, intrinsic correlation length [41, 42]. Disorder is expected to limit the divergence of the correlation length and the narrowing of the quasielastic peak as $T \to 0$, and hence to preclude the long-range ordered state that would be driven by interlayer exchange interactions or spin-space anisotropies in a clean system [1]. These factors are possible origins of the intensity reduction of the inelastic component as $\omega \to 0$ in the low-temperature data of figure 1. To summarize this section, we emphasize that the slow spin dynamics evidenced by figure 5 appears to be an intrinsic consequence of the nearly two-dimensional, nearly isotropic nature of the spin system. This picture is quite different from the 'spin glass' phenomenology of the underdoped cuprates, according to which this behavior reflects the randomness and frustration induced by the dopant atoms.

3.3.2. Electronic liquid crystal (ELC). At temperatures exceeding $T_{\mathrm{SDW}} \sim 40\,\mathrm{K}$, the quasi-elastic peak of figure 1 is no longer visible, but prominent low-energy incommensurate spin fluctuations persist. Since the incommensurability could not be resolved in most of the inelastic scattering profiles for $x \leqslant 0.35$, we have extracted the momentum widths (FWHM) of the profiles in the a^* and b^* directions, Δ_a and Δ_b, from scans like those shown in figure 2 at different temperatures. Whenever the incommensurate peak separation 2δ exceeded Δ_b, Δ_a was extracted from a two-Gaussian fit. Otherwise, the a^* scan was fitted by a single Gaussian for the sake of simplicity. For either way of fitting, Δ_a is the difference of the H values for which the intensity drops to half of the maximum intensity.

Figure 6 shows the resulting widths Δ_a and Δ_b, corrected for the instrumental resolution. While Δ_b increases gradually upon heating, Δ_a decreases and continuously approaches Δ_b. The temperature dependence of Δ_a was therefore fitted by a polynomial function, while for Δ_b a simple linear fit was applied that accounts for the thermal broadening of the peaks. The point of intersection of these two curves marks T_{ELC}, the onset temperature of the incommensurability. Above T_{ELC}, both widths are nearly identical and increase in a parallel manner upon further heating.

In order to compare the three different samples directly, we have plotted the temperature dependence of the anisotropy, defined as the deviation from unity of the ratio of Δ_a and the linear fit of Δ_b (figure 7). While the low-temperature limit of the anisotropy decreases with decreasing hole concentration, reflecting the doping dependence of the incommensurability (figure 2), the temperature where $\Delta_a/\Delta_b - 1 \to 0$ increases with decreasing p.

The strong temperature dependence of the in-plane anisotropy of the spin fluctuations in all three samples and its appearance at a well-defined, doping-dependent onset temperature confirms that this phenomenon arises from collective interactions between spins. The 'Ising nematic' transition expected on general grounds for a 2D incommensurate magnet ([21]; for reviews see [16, 43] and [44–48]) possibly associated with a 'Pomeranchuk' instability of the Fermi surface [48]–[50], provides an interesting qualitative explanation of our observations,

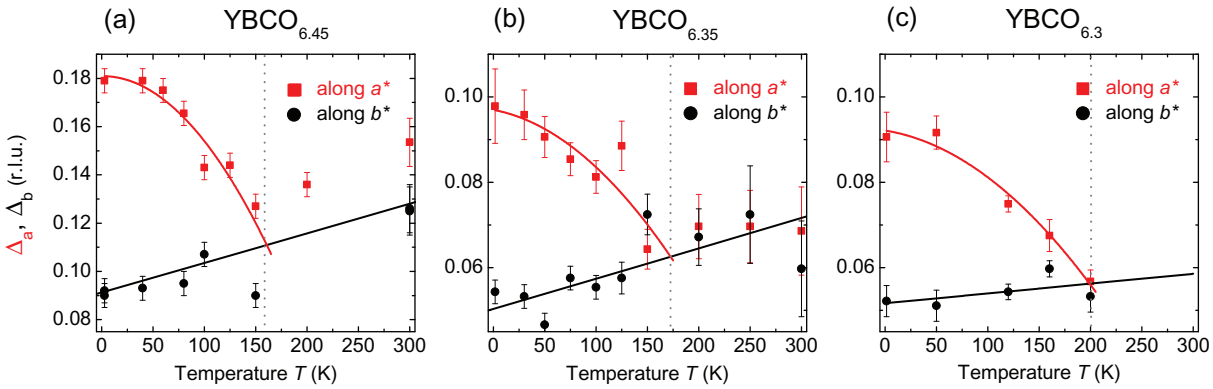

Figure 6. Temperature evolution of the effective momentum widths (FWHM) along the a- and b-direction of the spin excitation profiles at $E = 3$ meV for (a) $YBCO_{6.45}$ (b) $YBCO_{6.35}$ and (c) $YBCO_{6.3}$. The widths were extracted from constant-energy scans, as shown in figure 2, and corrected for the instrumental resolution.

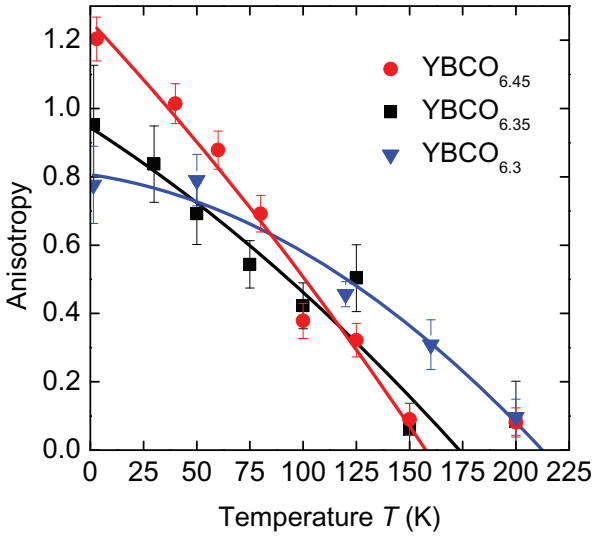

Figure 7. Comparison of the temperature-dependent anisotropy, $\Delta_a/\Delta_b - 1$, of the effective momentum widths Δ_a and Δ_b for $E = 3$ meV for the three different hole-doping levels. The temperature for which the polynomial fit yields $\Delta_a/\Delta_b - 1 = 0$ is defined as the ELC transition temperature T_{ELC}.

but a quantitative assessment of this scenario will have to await further theoretical progress. Meanwhile, it is interesting to compare our $YBCO_{6+x}$ data to analogous observations on the $Ba_2Fe_{2-x}(Co, Ni)_xAs_2$ system, where a strong, doping-dependent in-plane anisotropy of the spin excitations has also been found [51, 52]. In contrast to the cuprates, however, this anisotropy is temperature independent, at least in the superconducting regime of the phase diagram, and can be associated with nesting features of the Fermi surface [52]. The SDW and ELC states in $YBCO_{6+x}$, which are observed in the immediate vicinity of the Mott insulator, thus do not appear to be straightforwardly related to the more conventional SDW state in the iron pnictides.

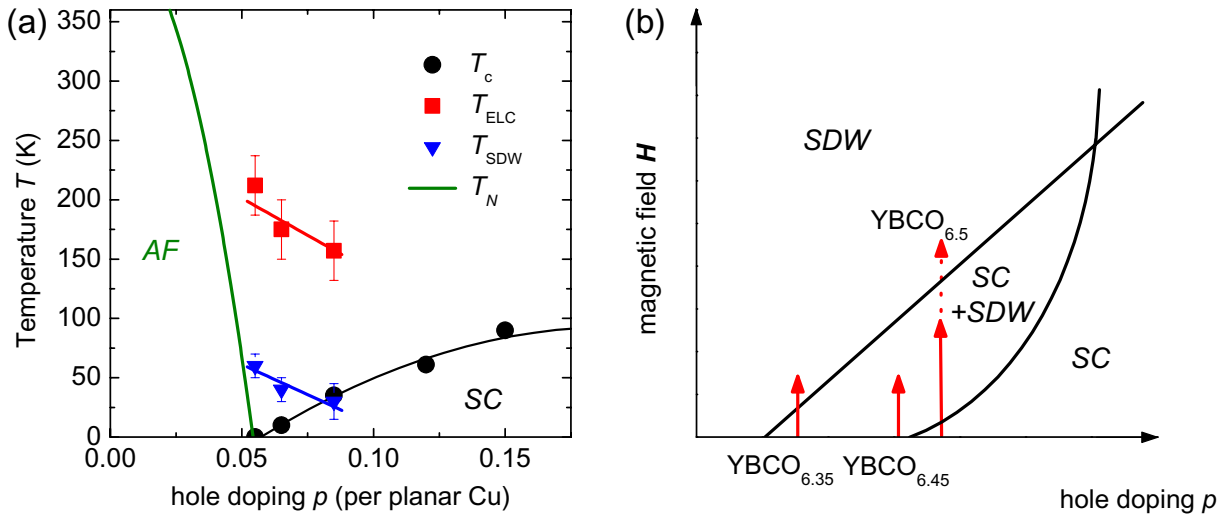

Figure 8. Magnetic phase diagram of underdoped $YBCO_{6+x}$. (a) A p–T section of the phase diagram with the crossover temperatures T_{SDW} and T_{ELC} extracted from figure 5(a) (and similar data for other samples) and figure 7, respectively, along with the phase boundaries of commensurate antiferromagnetism [22] and superconductivity [53]. (b) A schematic diagram of a p–**H** section of the phase diagram derived in a field-theoretical treatment of competing SDW and SC order parameters [35]. The control parameter in the field theory was heuristically identified with the doping level p. The field range covered by the data of figure 4 and the larger field range covered by the quantum oscillation experiments on $YBCO_{6.5}$ samples are indicated by red arrows.

4. Summary

Figure 8(a) summarizes the overall layout of the p–T phase diagram of underdoped $YBCO_{6+x}$. The SDW and ELC crossover lines established by our neutron scattering results are shown along with the previously determined phase boundaries for commensurate antiferromagnetism [22] and superconductivity [53]. At $T = 0$, the SDW and SC phases coexist over some range of p. Our data are consistent with μSR evidence of coexistence between magnetic order and superconductivity in this doping regime [22, 54], but μSR does not contain information about the spatial character of the local magnetization. The neutron scattering data presented here demonstrate that the magnetic order coexisting with superconductivity is incommensurate. At the present time, they are insufficient to determine whether the coexistence is spatially uniform, as predicted by spiral models [17, 30], or spatially modulated in the form of stripes [16, 55] or spin vortex lattices [56]. In any case, unavoidable oxygen defects in the $YBCO_{6+x}$ crystal lattice are expected to induce some degree of spatial inhomogeneity.

Both the SDW order parameter extracted from the intensity of the quasi-elastic peak as $T \to 0$ and the crossover temperature T_{SDW} that characterizes its onset at $T \neq 0$ are continuously reduced with increasing p. This indicates that the SDW phase boundary ends at a quantum critical point (QCP) at $p \sim 0.1$, close to the chemical composition $YBCO_{6.5}$. Further evidence for quantum criticality is derived from the scaling properties of the dynamical spin correlations

of $YBCO_{6.45}$ [57]. In line with this scenario, the scattering function at $T = 0$ exhibits a spin gap for $p > 0.1$ [58], but a dilute concentration of nonmagnetic impurities restores the SDW [29].

The low-p end of the incommensurate SDW regime is complicated by a confluence of several factors including the tetragonal-to-orthorhombic transition [26], the onset of appreciable effective interactions between CuO_2 bilayers ($\sim J_\perp \xi^2$, where $J_\perp \sim 0.02$ meV is the bare inter-bilayer interaction [1] and ξ is the intra-layer correlation length, which increases with decreasing p) and dopant-induced disorder, which may lead to the formation of local Cu^{2+} moments on the CuO chains for samples with low oxygen content [59]. Nonetheless, it is interesting to note that the onset of incommensurability in the spin correlations (figure 3) nearly coincides with the onset of superconductivity (figure 8). The $YBCO_{6+x}$ system is less dominated by disorder than strongly underdoped LSCO [60] and thus provides an interesting complementary forum for future exploration of the interplay between spin and charge correlations close to the Mott-insulating state.

In order to relate our low-temperature neutron scattering data to the results of the quantum oscillation experiments, we have schematically drawn the range of magnetic fields covered by our experiments on top of the zero-temperature phase diagram for coupled SDW and d-wave SC parameters derived from field theory [34] (figure 8(b)). Here, the control parameter in the field theory was heuristically identified with the hole concentration p, without claims to theoretical rigor or quantitative accuracy. Whereas $YBCO_{6.35}$ appears to be near the SDW end of the coexistence regime, far away from the QCP, both our $YBCO_{6.45}$ sample and the $YBCO_{6.5}$ samples used in the quantum oscillation experiments are close to the QCP. The limited magnetic fields currently available for neutron scattering are incapable of promoting the electron system into the uniform SDW phase expected at high $\mathbf{H}$, but sufficient to substantially increase the SDW order parameter in the coexistence regime. In models with uniform SDW–SC coexistence for $\mathbf{H} = 0$, this proceeds via a spatially periodic enhancement of the SDW order in the vicinity of magnetic vortices in the mixed state of the d-wave SC. It will be interesting to explore a possible relation between the spatially modulated SDW order and the series of field-induced transitions recently observed in the magnetic vortex lattice of optimally doped $YBCO_{6+x}$ [61]. The much higher fields used for the quantum oscillation experiments are expected to bring the electron system of samples with doping levels near the zero-field QCP either close to the high-field boundary of the SDW–SC coexistence range or into the uniform SDW phase (figure 8(b)). An extrapolation of our low-field measurements of the SDW order parameter of $YBCO_{6.45}$ to $\mathbf{H} = 50$ T yields $\sim 0.13\mu_B$ per Cu ion [18], comparable to the zero-field sublattice magnetization of stripe-ordered Nd- or Eu-substituted LSCO, where recent photoemission experiments have uncovered evidence of a reconstructed Fermi surface [62, 63]. It is thus likely that an SDW reconstruction of the multiband Fermi surface of $YBCO_{6.5}$ contributes to the formation of the small pockets observed in the quantum oscillation experiments. This conclusion is supported by recent quantitative assessments of the quantum oscillation data [19, 20]. It is interesting to note that the QCP indicated by our neutron scattering study coincides with the insulator–metal transition inferred from transport experiments in high magnetic fields [64, 65], and that the transport data indicate a critical divergence of the cyclotron mass at this doping level [65, 66]. A comprehensive explanation of the neutron-scattering and quantum-oscillation data therefore requires a transition from 'SDW insulator' to 'SDW metal' at high fields [67], for which there is so far no direct experimental evidence.

Going back to the zero-field phase diagram of figure 8(a), we note that the ELC onset temperature also increases with decreasing p, such that the ELC and SDW crossover

lines are nearly parallel. In view of the minute size ($\sim 0.5\%$ for $YBCO_{6.35}$) and opposite doping trend of the orthorhombic distortion of the crystal structure [26, 68], this observation supports our contention [15] that the anisotropy is not a simple consequence of the crystal symmetry [69], but arises spontaneously from many-body interactions between spins. The ELC onset temperature is substantially lower than the onset of the 'charge pseudogap' detected by infrared spectroscopy [25, 70, 71], which at these doping levels is well above room temperature. However, it coincides with the onset of signatures of phase-incoherent superconductivity in the infrared spectra of $YBCO_{6+x}$ samples from the same batch as ours [71]. The theoretical description of the subtle interplay between SC and spin correlations for $T \sim T_{ELC}$ is an interesting subject for further investigation, as is the relationship between the ELC phenomenon reported here and the spontaneous onset of in-plane anisotropies in dc resistivity [68] and Nernst effect [24] measurements. While the temperature evolution of the in-plane resistivity anisotropy [68] is in good qualitative agreement with the anisotropy of the spin dynamics shown in figure 7, corresponding Nernst-effect data are not yet available for the doping levels investigated here.

Finally, it will be important to follow the ELC crossover line to higher doping levels, where the SDW phase is no longer present at $T = 0$. For $YBCO_{6.6}$ ($p \sim 0.12$), the spin excitation spectrum exhibits a gap in the SC state at $T = 0$ [59]. Weak low-energy spin excitations are present above T_c, but their temperature dependence has not yet been studied in detail. The intensity of higher-energy excitations with $E \sim 30$ meV, however, shows a strong upturn upon cooling below ~ 150 K [72], in qualitative agreement with transport [24, 68] and infrared [71] data. Taken together, these results suggest that the ELC phenomenon persists at least up to $p \sim 0.12$. It will be interesting to explore the relationship between this transition and the 'spin pseudogap' detected by nuclear magnetic resonance [73], polar Kerr effect measurements indicating the presence of a broken-symmetry state [74] as well as the magnetic reflections with $\mathbf{Q} = 0$ detected by elastic neutron scattering [75, 76] in this doping regime.

Acknowledgments

We thank O Sushkov, G Khaliullin, C Bernhard, Ch Niedermayer, A Dubroka, Y Pashkevich, D Inosov, Y Li and S Kivelson for discussions, S Lacher, B Baum and H Wendel for their help with sample preparation, C Busch and H Bender for technical support and C Stefani and R Dinnebier for determining the lattice parameters using x-ray powder diffraction. We acknowledge financial support from the DFG under grant no. FOR538.

References

[1] Tranquada J M, Shirane G, Keimer B, Shamoto S and Sato M 1989 Neutron scattering study of magnetic excitations in $YBa_2Cu_3O_{6+x}$ *Phys. Rev.* B **40** 4503

[2] Coldea R, Hayden S M, Aeppli G, Perring T G, Frost C D, Mason T E, Cheong S-W and Fisk Z 2001 Spin waves and electronic interactions in La_2CuO_4 *Phys. Rev. Lett.* **86** 5377

[3] Proust C, Boaknin E, Hill R W, Taillefer L and Mackenzie A P 2002 Heat transport in a strongly overdoped cuprate: Fermi liquid and a pure d-wave BCS superconductor *Phys. Rev. Lett.* **89** 147003

[4] Nakamae S, Behnia K, Mangkorntong N, Nohara M, Takagi H, Yates S J C and Hussey N E 2003 Electronic ground state of heavily overdoped nonsuperconducting $La_{2-x}Sr_xCuO_4$ *Phys. Rev.* B **68** 100502

[5] Vignolle B, Carrington A, Cooper R A, French M M J, Mackenzie A P, Jaudet C, Vignolles D, Proust C and Hussey N E 2008 Quantum oscillations in an overdoped high-T_c superconductor *Nature* **455** 952

[6] Doiron-Leyraud N, Proust C, LeBoeuf D, Levallois J, Bonnemaison J-B, Liang R, Bonn D A, Hardy W N and Taillefer L 2007 Quantum oscillations and the Fermi surface in an underdoped high-T_c superconductor *Nature* **447** 565

[7] LeBoeuf D *et al* 2007 Electron pockets in the Fermi surface of hole-doped high-T_c superconductors *Nature* **440** 533

[8] Yelland E A, Singleton J, Mielke C H, Harrison N, Balakirev F F, Dabrowski B and Cooper J R 2008 Quantum oscillations in the underdoped cuprate $YBa_2Cu_4O_8$ *Phys. Rev. Lett.* **100** 047003

[9] Bangura A F *et al* 2008 Small Fermi surface pockets in underdoped high temperature superconductors: observation of Shubnikov–de Haas oscillations in $YBa_2Cu_4O_8$ *Phys. Rev. Lett.* **100** 047004

[10] Sebastian S E, Harrison N, Palm E, Murphy T P, Mielke C H, Liang R, Bonn D A, Hardy W N and Lonzarich G G 2008 A multi-component Fermi surface in the vortex state of an underdoped high-T_c superconductor *Nature* **454** 200

[11] Yamada K *et al* 1998 Doping dependence of the spatially modulated dynamical spin correlations and the superconducting-transition temperature in $La_{2-x}Sr_xCuO_4$ *Phys. Rev.* B **57** 6165

[12] Fujita M, Yamada K, Hiraka H, Gehring P M, Lee S H, Wakimoto S and Shirane G 2002 Static magnetic correlations near the insulating-superconducting phase boundary in $La_{2-x}Sr_xCuO_4$ *Phys. Rev.* B **65** 064505

[13] Wakimoto S *et al* 1999 Observation of incommensurate magnetic correlations at the lower critical concentration for superconductivity in $La_{2-x}Sr_xCuO_4$ ($x = 0.05$) *Phys. Rev.* B **60** R769

[14] Wakimoto S *et al* 2000 Direct observation of a one-dimensional static spin modulation in insulating $La_{1.95}Sr_{0.05}CuO_4$ *Phys. Rev.* B **61** 3699

[15] Hinkov V, Haug D, Fauqué B, Bourges P, Sidis Y, Ivanov A, Bernhard C, Lin C T and Keimer B 2008 Electronic liquid crystal state in the high-temperature superconductor $YBa_2Cu_3O_{6.45}$ *Science* **319** 597

[16] Kivelson S A, Bindloss I P, Fradkin E, Oganesyan V, Tranquada J M, Kapitulnik A and Howald C 2003 How to detect fluctuating stripes in the high-temperature superconductors *Rev. Mod. Phys.* **75** 1201

[17] Kotov N V and Sushkov O P 2005 Theory of anisotropic hopping transport due to spiral correlations in the spin-glass phase of underdoped cuprate superconductors *Phys. Rev.* B **72** 184519

[18] Haug D *et al* 2009 Magnetic-field-enhanced incommensurate magnetic order in the underdoped high-temperature superconductor $YBa_2Cu_3O_{6.45}$ *Phys. Rev. Lett.* **103** 017001

[19] Harrison N 2009 Spin-density wave Fermi surface reconstruction in underdoped $YBa_2Cu_3O_{6+x}$ *Phys. Rev. Lett.* **102** 206405

[20] Sebastian S E, Harrison N, Goddard P A, Altarawneh M M, Mielke C H, Liang R, Bonn D A, Hardy W N, Andersen O K and Lonzarich G G 2010 Compensated electron and hole pockets in an underdoped high-T_c superconductor *Phys. Rev.* B **81** 214524

[21] Kivelson S A, Fradkin E and Emery V J 1998 Electronic liquid-crystal phases of a doped Mott insulator *Nature* **393** 550

[22] Coneri F, Sanna S, Zheng K, Lord J and De Renzi R 2010 Magnetic states of lightly hole-doped cuprates in the clean limit as seen via zero-field muon spin spectroscopy *Phys. Rev.* B **81** 104507

[23] Wang Y, Li L and Ong N P 2006 Nernst effect in high-T_c superconductors *Phys. Rev.* B **73** 024510

[24] Daou R *et al* 2010 Broken rotational symmetry in the pseudogap phase of a high-T_c superconductor *Nature* **463** 519

[25] Timusk T and Statt B 1999 The pseudogap in high-temperature superconductors: an experimental survey *Rep. Prog. Phys.* **62** 61

[26] Jorgensen J D, Veal B W, Paulikas A P, Nowicki L J, Crabtree G W, Claus H and Kwok W K 1990 Structural properties of oxygen-deficient $YBa_2Cu_3O_{7-\delta}$ *Phys. Rev.* B **41** 1863

[27] Liang R, Bonn D A and Hardy W N 2006 Evaluation of CuO_2 plane hole doping in $YBCO_{6+x}$ single crystals *Phys. Rev.* B **73** 180505

[28] Bayrakci S P, Keller T, Habicht K and Keimer B 2006 Spin-wave lifetimes throughout the Brillouin zone *Science* **312** 1926

[29] Suchaneck A *et al* 2010 Incommensurate magnetic order and dynamics induced by spinless impurities in $YBa_2Cu_3O_{6.6}$ *Phys. Rev. Lett.* **105** 037207

[30] Sushkov O P 2009 Spin spirals in underdoped $La_{2-x}Sr_xCuO_4$ and $YBa_2Cu_3O_{6+y}$: differences and similarities *Phys. Rev.* B **79** 174519
[31] Chen W, Sushkov O P and Tohyama T 2010 Magnetic quantum oscillations and multiple holon pockets in the underdoped cuprates $YBa_2Cu_3O_{6+y}$ *Phys. Rev.* B **82** 060511
[32] Katano S, Sato M, Yamada K, Suzuki T and Fukase T 2000 Enhancement of static antiferromagnetic correlations by magnetic field in a superconductor $La_{2-x}Sr_xCuO_4$ with $x = 0.12$ *Phys. Rev.* B **62** R14677
[33] Lake B *et al* 2002 Antiferromagnetic order induced by an applied magnetic field in a high-temperature superconductor *Nature* **415** 299
[34] Khaykovich B, Wakimoto S, Birgeneau R J, Kastner M A, Lee Y S, Smeibidl P, Vorderwisch P and Yamada K 2005 Field-induced transition between magnetically disordered and ordered phases in underdoped $La_{2-x}Sr_xCuO_4$ *Phys. Rev.* B **71** 220508
[35] Demler E, Sachdev S and Zhang Y 2001 Spin-ordering quantum transitions of superconductors in a magnetic field *Phys. Rev. Lett.* **87** 067202
[36] Stock C, Buyers W J L, Rule K C, Chung J-H, Liang R, Bonn D and Hardy W N 2009 Magnetic field resonantly enhanced free spins in heavily underdoped $YBa_2Cu_3O_{6+x}$ *Phys. Rev.* B **79** 184514
[37] Chang J *et al* 2008 Tuning competing orders in $La_{2-x}Sr_xCuO_4$ cuprate superconductors by the application of an external magnetic field *Phys. Rev.* B **78** 104525
[38] Niedermayer C, Bernhard C, Blasius T, Golnik A, Moodenbaugh A and Budnick J I 1998 Common phase diagram for antiferromagnetism in $La_{2-x}Sr_xCuO_4$ and $Y_{1-x}Ca_xBa_2Cu_3O_6$ as seen by muon spin rotation *Phys. Rev. Lett.* **80** 3843
[39] Sternlieb B J *et al* 1990 Muon-spin-relaxation and neutron-scattering studies of magnetism in single-crystal $La_{1.94}Sr_{0.06}CuO_4$ *Phys. Rev.* B **41** 8866
[40] Keimer B *et al* 1992 Magnetic excitations in pure, lightly doped, and weakly metallic La_2CuO_4 *Phys. Rev.* B **46** 14034
[41] Auerbach A and Arovas D P 1988 Spin dynamics in the square-lattice antiferromagnet *Phys. Rev. Lett.* **61** 617
[42] Katanin A A and Sushkov O P 2010 Quasielastic neutron scattering from two dimensional antiferromagnets at a finite temperature arXiv:1008.2562
[43] Vojta M 2009 Lattice symmetry breaking in cuprate superconductors: stripes, nematics, and superconductivity *Adv. Phys.* **58** 699
[44] Oganesyan Y, Kivelson S A and Fradkin E 2010 Quantum theory of a nematic Fermi fluid *Phys. Rev.* B **64** 195109
[45] Kee H-Y, Kim E H and Chung C-H 2003 Signatures of an electronic nematic phase at the isotropic–nematic phase transition *Phys. Rev.* B **68** 245109
[46] Huh Y and Sachdev S 2008 Renormalization group theory of nematic ordering in d-wave superconductors *Phys. Rev.* B **78** 064512
[47] Sun K, Lawler M J and Kim E-A 2010 Spin-charge interplay in electronic liquid crystals: fluctuating spin stripe driven by charge nematic ordering *Phys. Rev. Lett.* **104** 106405
[48] Halboth C J and Metzner W 2000 d-Wave superconductivity and Pomeranchuk instability in the two-dimensional Hubbard model *Phys. Rev. Lett.* **85** 5162
[49] Yamase H and Kohno H 2000 Possible quasi-one-dimensional Fermi surface in $La_{2-x}Sr_xCuO_4$ *J. Phys. Soc. Japan* **69** 332
[50] Yamase H 2009 Spontaneous Fermi surface symmetry breaking in bilayer systems *Phys. Rev.* B **80** 115102
[51] Lester C, Chu J-H, Analytis J G, Perring T G, Fisher I R and Hayden S M 2010 Dispersive spin fluctuations in the nearly optimally doped superconductor $Ba(Fe_{1-x}Co_x)_2As_2$ ($x = 0.065$) *Phys. Rev.* B **81** 064505
[52] Park J T *et al* 2010 Symmetry of spin excitation spectra in the tetragonal paramagnetic and superconducting phases of 122-ferropnictides *Phys. Rev.* B **82** 134503
[53] Liang R, Bonn D A, Hardy W N and Broun D 2005 Lower critical field and superfluid density of highly underdoped $YBa_2Cu_3O_{6+x}$ single crystals *Phys. Rev. Lett.* **94** 117001

[54] Miller R I, Kiefl R F, Brewer J H, Callaghan F D, Sonier J E, Liang R, Bonn D A and Hardy W 2006 Coexistence of magnetism and superconductivity in ultraclean underdoped $YBa_2Cu_3O_{6.37}$ *Phys. Rev.* B **73** 144509

[55] Berg E, Fradkin E, Kim E-A, Kivelson S A, Oganesyan V, Tranquada J M and Zhang S C 2007 Dynamical layer decoupling in a stripe-ordered high-T_c superconductor *Phys. Rev. Lett.* **99** 127003

[56] Fine B V 2007 Magnetic vortices instead of stripes: another interpretation of magnetic neutron scattering in lanthanum cuprates *Phys. Rev.* B **75** 060504

[57] Hinkov V *et al* 2010 unpublished data

[58] Fong H F, Bourges P, Sidis Y, Regnault L P, Bossy J, Ivanov A, Milius D L, Aksay I A and Keimer B 2000 Spin susceptibility in underdoped $YBa_2Cu_3O_{6+x}$ *Phys. Rev.* B **61** 14773

[59] Kadowaki H, Nishi N, Yamada K, Takeya H, Takei H, Shapiro S M and Shirane G 1988 Successive magnetic phase transitions in tetragonal $YBCO_{6+x}$ *Phys. Rev.* B **37** 7932

[60] Chen W, Khaliullin G and Sushkov O P 2009 Coulomb disorder effects on angle-resolved photoemission and nuclear quadrupole resonance spectra in cuprates *Phys. Rev.* B **80** 094519

[61] White J S *et al* 2009 Fermi surface and order parameter driven vortex lattice structure transitions in twin-free $YBa_2Cu_3O_7$ *Phys. Rev. Lett.* **102** 097001

[62] Chang J *et al* 2008 Electronic structure near the 1/8-anomaly in La-based cuprates *New J. Phys.* **10** 103016

[63] Zabolotnyy V B *et al* 2009 Evidence for Fermi surface reconstruction in the static stripe phase of $La_{1.8-x}Eu_{0.2}Sr_xCuO_4$, $x = 1/8$ *Europhys. Lett.* **86** 47005

[64] Sun X F, Segawa K and Ando Y 2004 Metal-to-insulator crossover in $YBa_2Cu_3O_y$ probed by low-temperature quasiparticle heat transport *Phys. Rev. Lett.* **93** 107001

[65] Sebastian S E, Harrison, Altarawneh M M, Mielke C H, Liang R, Bonn D A and Lonzarich G G 2010 Metal–insulator quantum critical point beneath the high T_c superconducting dome *Proc. Natl Acad. Sci. USA* **107** 6175

[66] Norman M R, Lin J and Millis A J 2010 Lifshitz transition in underdoped cuprates *Phys. Rev.* B **81** 180513

[67] Sachdev S 2010 Quantum phase transitions of antiferromagnets and the cuprate superconductors arXiv:1002.3823

[68] Ando Y, Segawa K, Komiya S and Lavrov A N 2002 Electrical resistivity anisotropy from self-organized one dimensionality in high-temperature superconductors *Phys. Rev. Lett.* **88** 137005

[69] Singh D J and Mazin I I 2010 Experimental evidence for nematic order of cuprates in relation to lattice structure arXiv:1007.0255

[70] Yu L, Munzar D, Boris A V, Yordanov P, Chaloupka J, Wolf T, Lin C T, Keimer B and Bernhard C 2008 Evidence for two separate energy gaps in underdoped high-temperature cuprate superconductors from broadband infrared ellipsometry *Phys. Rev. Lett.* **100** 177004

[71] Dubroka A *et al* 2010 Evidence of precursor superconductivity as high as 180 K from infrared spectroscopy arXiv:1009.2925

[72] Hinkov V, Bourges P, Pailhès S, Sidis Y, Ivanov A, Frost C D, Perring T G, Lin C T, Chen D P and Keimer B 2007 Spin dynamics in the pseudogap state of a high-temperature superconductor *Nat. Phys.* **3** 780

[73] For a review see Alloul H, Bobroff J, Gabay M and Hirschfeld P J 2009 Defects in correlated metals and superconductors *Rev. Mod. Phys.* **81** 45

[74] Xia J *et al* 2008 Polar Kerr-Effect Measurements of the High-Temperature $YBa_2Cu_3O_{6+x}$ Superconductor: Evidence for Broken Symmetry near the Pseudogap Temperature *Phys. Rev. Lett.* **100** 127002

[75] Fauqué B, Sidis Y, Hinkov V, Pailhès S, Lin C T, Chaud X and Bourges P 2006 Magnetic order in the pseudogap phase of high-T_c superconductors *Phys. Rev. Lett.* **96** 197001

[76] Mook H A, Sidis Y, Fauqué B, Balédent V and Bourges P 2008 Observation of magnetic order in a superconducting $YBa_2Cu_3O_{6.6}$ single crystal using polarized neutron scattering *Phys. Rev.* B **78** 020506